# Three-dimensional numerical simulation for various geometries of solid oxide fuel cells

J.R. Ferguson[1], J.M. Fiard[2], and R. Herbin[3]

**Abstract** A 3D mathematical model of a Solid Oxide Fuel Cell is presented here, which allows the computation of the local distributions of the electrical potential, the temperature and the concentrations of the chemical species. The physics of the cell and the simplifying assumptions are presented, and a sketch of the numerical procedure is given. The numerical results obtained with hydrogen as the fuel are compared with results from other simulation codes which were developed for a planar geometry. The numerical results show the behaviour of the potential, temperature and current distributions when certain parameters (geometry of the cell, electrolyte materials, temperature in the channels) are varied. Numerical simulation is also used to obtain an optimum for some geometry parameters such as cathode thickness or rib width.

## 1 Introduction

The work presented here deals with the mathematical modelling and numerical simulation of natural gas-fed solid oxide cells (Solid Oxide Fuel Cell, SOFC) at a stationary regime. The principle of a Solid Oxide Fuel Cell (SOFC) is based on the conversion of the chemical energy which is stored in the fuel (hydrogen or methane) into electrical energy through an electron-producing electrochemical reaction (see e.g. [4]). The electrical energy produced by an electrochemical reaction depends on the reacting species concentrations through the Nernst law. A schematic diagram of the electrochemical processes is given in Figure 1; these are that:

1. oxygen diffuses through the porous cathode material.
2. oxygen molecules are dissociated and ionized at the cathode/electrolyte interface.
3. oxygen ions migrate through the electrolyte towards the anode/electrolyte interface.
4. fuel diffuses through the porous anode material.
5. hydrogen contained in (and/or produced by) the fuel reacts with the oxygen ions, producing water and liberating electrons, which flow back to the cathode/electrolyte interface, via an external circuit.

Hydrogen can be produced from methane, and an interesting feature of a solid oxide fuel cell is the fact that it runs at a temperature which is sufficiently high to allow internal reforming, which is taken into account in the present model. The SOFC systems seem to be of great interest for use of natural gas, because of their high power generation and heat recovery efficiency, as well as their low pollution rate. Moreover, the electrolyte in a SOFC is solid rather than liquid (as for instance in a phosphoric acid fuel cell) and therefore there is no need to handle corrosive liquids. Because of their high temperature operating conditions, internal reforming of methane is possible, along with heat generation from the hot steam which is produced by the cell. However, the ideal efficiency rate is never attained in experimental conditions. Important losses seem to be internal ohmic losses; diffusion losses and overpotential due to the electrochemical reactions can also be expected. The aim of the mathematical modelling and numerical simulation of such a system is to give, for a given set of data describing the geometry of the cell and the operating conditions, an estimate of these losses and where they occur. Also, by varying the set of input parameters describing either the geometry or the operating conditions, the influence of these parameters on the efficiency of the cell can be studied. Hence modelling may be viewed as a design tool.

[1] Ennetbaden, Switzerland
[2] Program in Applied Mathematics, UC Boulder, CO 80309-0526, USA.
[3] CMI, Université de Provence, 13453 Marseille 13, France.

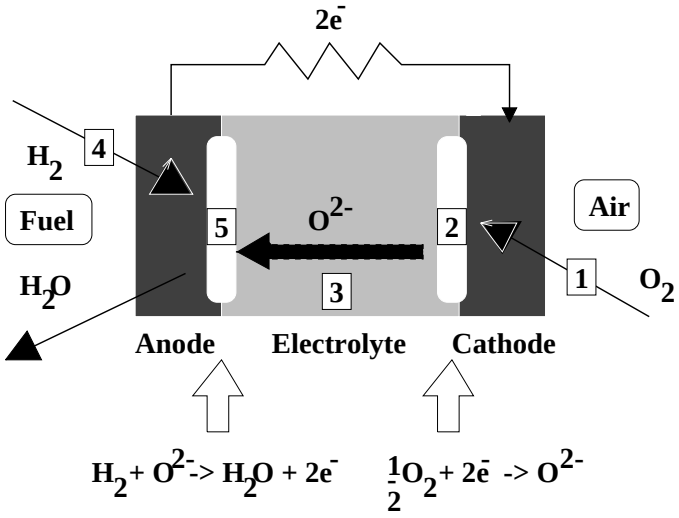


Figure 1: Electrochemical processes in a SOFC

Numerical simulation of SOFCs has already been performed with mathematical models which were obtained with some simplifying assumptions (see [29], [14] and references therein). A 2D mathematical model of a cross-section of a planar solid oxide fuel cell was also developed [15], [16]; in these works as in the present work, the distributions of temperature, species concentrations and electrical current are obtained within the unit cell itself, whereas in other works which are concerned with the modelling of a whole stack, the solid materials were assumed to be all at the same temperature and the current density was computed by averaging the conductivities of the various components [10], [1], [28]. A number of models of the unit cell also exist which were tested on a benchmark defined in an IEA workshop [2]. The originality of the present work lies in the fact that it yields the local distribution of temperature, electric potential and concentrations in a three-dimensional unit cell for various geometries, and it uses a flux-conservative discretization scheme, the "finite volume" scheme, (see e.g. [27], [12]) to do so.

The following sections are organized as follows: section 2 is devoted to the description of the geometry of a unit cell, and, more precisely, to the geometries which have already been implemented in the numerical code. Section 3 deals with the mathematical model itself, i.e the governing equations and the boundary conditions which were discretized in order to compute the local distributions. Section 4 describes the numerical procedure and the computer code which uses it. The validation of the code is demonstrated in section 5 by running it with the data of the benchmark defined in an IEA Workshop [2] and comparing it with other numerical codes. In section 6, we show how the numerical code can be viewed as a design tool; first the efficiencies of the parallel and cross-flow cases are compared. Then the influence of the electrode thickness on the efficiency of the cell is studied. In the case of internal reforming, an optimum value of the anode thickness can be computed. Finally, numerical results for cylindrical and tubular geometries are shown.

## 2 Description of the geometry

The SOFC system is in fact a stack of electrochemical cells, i.e. it is made up of several repeating "unit cells". The layout of the mathematical equations describing the physical and chemical phenomena can be carried out on the smallest non-repeating geometrical pattern which represents the unit cell. Several concepts exist for SOFC's, based on the geometry and the materials used for the different components of the cell. One of these concepts is the so-called "planar bi-polar" geometry (see Figure 2). This concept includes the "co-flow" and "counter-flow" where the air and gas channels are parallel, and the "cross-flow" case where

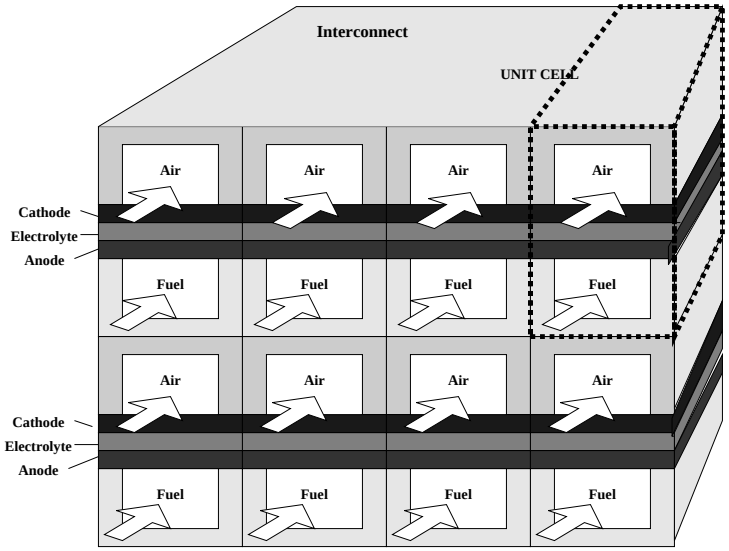


Figure 2: The planar concept for SOFCs

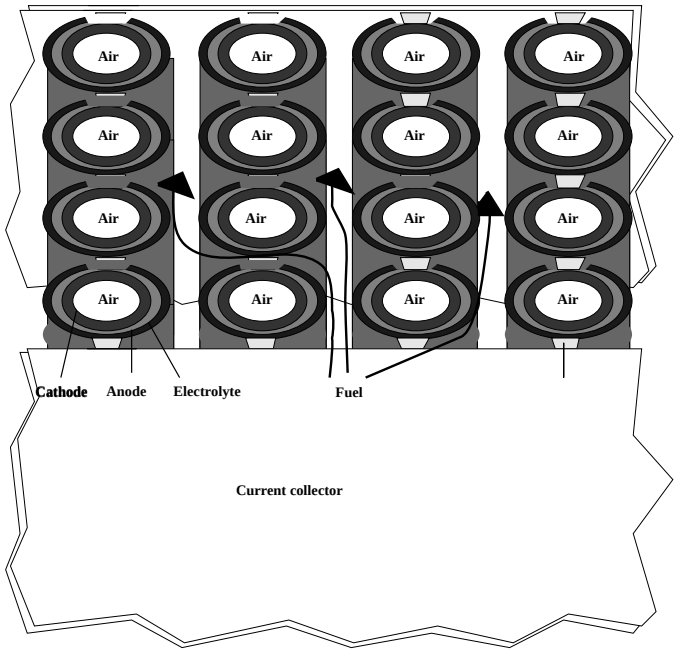


Figure 3: The tubular concept for SOFCs

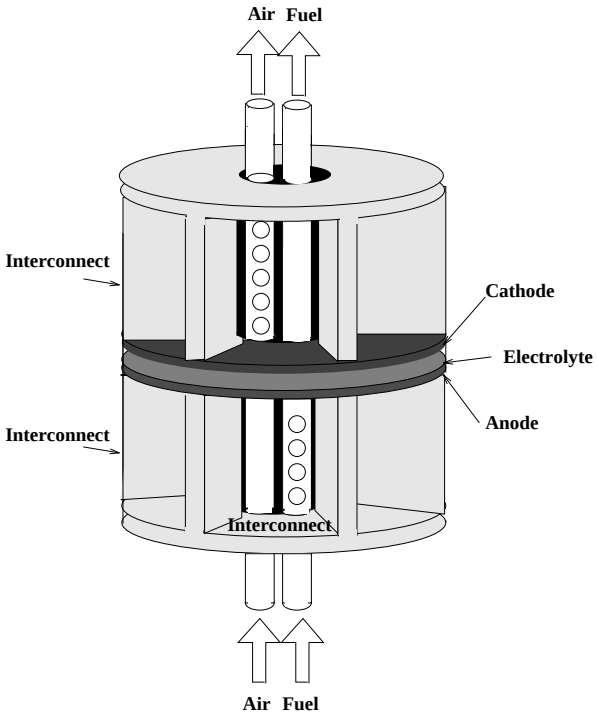


Figure 4: The cylindrical concept for SOFCs

the channels are perpendicular. The latter case is preferred by industry because of the simplicity of the manifolding.

The results of [14], which are based on a one dimensional model along the channel direction (i.e. 2D model in the case of a cross-flow configuration) indicate that the co-flow geometry should be the most efficient. This is also the case in the model developed by [24]. In a previous paper [17], the model of a cross-section of parallel flow configuration was developed. This model is generalized here for a 3D unit cell; the geometries which are considered are the planar concept, with co- counter- or cross-flow designs; our numerical code can also handle the tubular concept developed by Westinghouse, depicted in Figure 3 and the cylindrical geometry which is sketched in Figure 4; the code is also designed to be able to treat other geometries if needed. The unit cell mathematical model is independent of the cell geometry. It has to be formulated before carrying out the numerical computations which will yield the behaviour of the physical entities for one unit cell. It can also be used to compute the same physical entities for a whole stack provided that the stack is made up of the same repeating unit cells, and that the boundary conditions at the channel walls are independent of the cells (i.e. same concentrations of species and same temperatures), with adequate boundary conditions on the exterior of the stack (thermal and electrical insulation). For the sake of clarity, we describe the various parameters on a planar bi-polar co- or counter-flow geometry in Figure 5. The cell is built around a PEN (Positive electrode-Electrolyte-Negative electrode) sandwich, where the electrochemical processes occur. The interconnect material, denoted by $I$, supports the structure and also serves as the current collector. It is assumed to be made of a non-porous material. Hence the diffusion of oxygen only takes place through the cathode, denoted by $C$. The fuel which is used in a SOFC is methane; it diffuses through the porous anode, $A$, and is transformed into hydrogen by a series of chemical reactions, known as reforming, in the presence of a catalyst, throughout the anode, $A$. Let $E$ denote the electrolyte and $\Omega_S$ denote the solid part of the domain of study (i.e. anode, cathode, electrolyte and interconnect). Let $\mathrm{Ch_f}$ (resp. $\mathrm{Ch_a}$) denote the fuel (resp. air) channel. Note that in a two-dimensional model of a cross-section, the temperature and concentrations are assumed to be given in $\mathrm{Ch_f}$ and $\mathrm{Ch_a}$, and therefore the domain of study is $\Omega_S$ only (see [17]). The respective boundaries of these channels will be denoted $\Gamma_{\mathrm{Ch_a}}$ and $\Gamma_{\mathrm{Ch_f}}$.

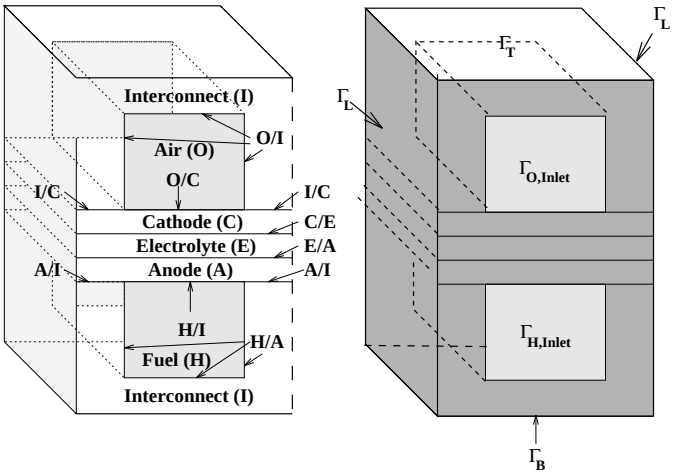


Figure 5: Geometry of a unit cell

In the case of tubular concept, the definition of the interfaces must be somewhat altered to take into account the fact that the electrolyte is insulated from the interconnect; the associated interface conditions are, however, quite easy to implement.

# 3 The mathematical model of a unit cell

## 3.1 Conservation laws

Let $\Phi$ denote the electric potential, $T$ the temperature and $X_i$ the molar concentration of species $i$ ($i = O_2$, $N_2$, $H_2$, $H_2O$, $CO$, $CO_2$, $CH_4$). The potential $\Phi$ is defined throughout $\Omega_S$, and continuous everywhere except at the electrode/electrolyte interfaces C/E and E/A; the temperature $T$ is defined and continuous throughout $\Omega_S$. The oxygen molar fraction $X_{O_2}$ (resp. the molar fractions $X_i$ i=$H_2$, $H_2O$, $CO$, $CO_2$, $CH_4$) is defined and continuous in the cathode C (resp. the anode A). The mathematical model is obtained by writing the conservation laws for the heat flux $\mathbf{q}$, the electric current $\mathbf{j}$ and the mass flux $\mathbf{N}_i$, $i = O_2$, $N_2$, $H_2$, $H_2O$, $CO$, $CO_2$, $CH_4$:

$$\begin{aligned}
\operatorname{div}(\mathbf{j}) &= 0 \text{ in I, C, E and A} && (1)\\
\operatorname{div}(\mathbf{q}) &= Q \text{ in I, C, E, A Ch}_\text{a} \text{ and Ch}_\text{f} && (2)\\
\operatorname{div}(\mathbf{N}_i) &= 0 \text{ for } i = O_2, N_2 \text{ in C and Ch}_\text{a} && (3)\\
\operatorname{div}(\mathbf{N}_i) &= r_i, \text{for } i = H_2, H_2O, CO, CO_2 \text{ and } CH_4 \text{ in A and Ch}_\text{f} && (4)
\end{aligned}$$

where $\operatorname{div}\mathbf{g} = \dfrac{\partial g_1}{\partial \mathrm{x}} + \dfrac{\partial g_2}{\partial \mathrm{y}} + \dfrac{\partial g_3}{\partial \mathrm{z}}$ for any vector valued function $g = \left(g_1, g_2, g_3\right)^T$, x, y, z representing the three space coordinates. $Q$ denotes the heat source term (arising from the passage of electric current and from the chemical reactions), and $r_i$ is the production rate of species $i$. There is now need to relate the fluxes $\mathbf{q}$, $\mathbf{j}$, $\mathbf{N}_i$ and the source terms $Q$ and $r_i$ with the unknowns $T$, $\Phi$ and $X_i$.

In the above equations, it is assumed that:

1. the electro-chemical reactions occur at the anode-electrolyte and cathode- electrolyte interfaces (i.e. heterogeneous reactions),
2. no chemical reactions occur within the air channel and
3. reforming and water-shift reactions occur within the fuel channel and anode domains.

## 3.2 Constitutive laws

In the solid parts, the thermal flux is mainly conductive, and modelled by Fourier's law of heat conduction:

$$\mathbf{q} = -\lambda \mathbf{grad}\ T \text{ in I, A, E and C,} \tag{5}$$

where $\mathbf{grad}\ T$ denotes the gradient of a scalar function $T$: $\mathbf{grad}\ T = \left(\frac{\partial T}{\partial \mathrm{x}}, \frac{\partial T}{\partial \mathrm{y}}, \frac{\partial T}{\partial \mathrm{z}}\right)^T$, and $\lambda$ is the thermal conductivity.
In the gas channels, the thermal flux is mainly convective in the gas flow direction, and conductive from the channel to the solid parts. Hence the expression of the flux:

$$\mathbf{q} = \sum_{i \in \mathcal{G}} C_{p\,i} \mathbf{N}_i T - \lambda \mathbf{grad}\ T \text{ in Ch}_\mathrm{f} \text{ and Ch}_\mathrm{a}, \tag{6}$$

where $\mathcal{G}$ denotes the set of various components of the gas mixtures, i.e. $\mathcal{G} = \{\ H_2,\ H_2O,\ CO,\ CO_2,\ CH_4\ \}$ in $\mathrm{Ch_f}$, whereas $\mathcal{G} = \{\ O_2,\ N_2\ \}$ in $\mathrm{Ch_a}$. The electric current is modelled by Ohm's law:

$$\mathbf{j} = -\sigma \mathbf{grad}\ \Phi \text{ in I, A, E and C,} \tag{7}$$

where $\sigma$ is the (temperature dependent) electric conductivity.
In the porous media (i.e. cathode and anode), the molar fluxes are mainly due to diffusion and satisfy Fick's law of diffusion in a mixture (see e.g. [8]):

$$\mathbf{N}_i = -cD_{i,mix} \mathbf{grad}\ X_i + X_i \sum_{j \in \mathcal{G}} \mathbf{N}_j \text{ in A and C,} \tag{8}$$

where $c$ is the concentration and $D_{i,mix}$ the diffusion coefficient of species $i$ in the considered mixture. In the gas channels, the molar flux is mainly convective in the flow direction and due to molecular diffusion at the boundaries $\Gamma_{\mathrm{Ch_f}}$ and $\Gamma_{\mathrm{Ch_a}}$, where the mass exchange may be taken into account using a mass transfer coefficient (see next section on boundary and interface conditions). Hence the molar flux may be written as:

$$\mathbf{N}_i = -cV_k X_i \text{ in } k, \text{ for } k = \mathrm{Ch_a} \text{ and } \mathrm{Ch_f}, \text{ for i} = \mathrm{O_2, N_2, H_2, H_2O, CO, CO_2, CH_4}. \tag{9}$$

where $V_k$ is the velocity of the mixture in channel $k$. In fact, we make the additional assumption that the nitrogen flux is zero in the air channel and porous cathode in any channel cross section.

## 3.3 Source terms

The volumetric heat source term $Q$ is in fact the sum of two terms. The first term is the ohmic heat source term and can be written $\sigma \mathbf{grad}\,\Phi \mathbf{grad}\,\Phi$. The second term is the heat produced by the shift and reforming reactions which take place in the porous, catalytic anode, and we shall denote it by $Q_{chem}$. The shift reaction:

$$CO + H_2O \leftrightarrow CO_2 + H_2 \tag{10}$$

is assumed to be in equilibrium. The heat produced is equal to the term $\Delta H_S$ of the reaction; the shift reaction occurs in both the porous anode and the fuel channel. The reforming reaction

$$CH_4 + H_2O \leftrightarrow 3H_2 + CO \tag{11}$$

is irreversible and thus the heat produced is equal to the enthalpy $\Delta H_R$. Finally, the heat source term can be expressed as:

$$Q = \sigma \mathbf{grad}\,\Phi \mathbf{grad}\,\Phi + Q_{chem} \tag{12}$$

$$Q_{chem} = \begin{cases} \Delta H_S \text{ in Ch}_\mathrm{f}, \\ \Delta H_S + \Delta H_R \text{ in } A, \\ 0 \text{ elsewhere.} \end{cases} \tag{13}$$

The volumetric mass source term $r_i$ is made of two terms :

$$r_i = \nu^S r^S + \nu^R r^R \tag{14}$$

where $r^S$ (resp. $r^R$) is the volumetric reaction rate of the reaction (10) (resp. (11)) and $\nu^S$ the stoechiometric coefficient of the reaction (10) (resp. (11)). The expression of $r^R$ was taken from the work of Lee [23]:

$$r^R = \rho\, k_0\, e^{(-E^R/(\mathrm{R}\ T))} P_{CH_4}^{\alpha} P_{H_2O}^{\beta} \tag{15}$$

where $\rho$ is the resistivity of the anode, $k_0$ the frequency factor, $E^R$ the activation energy of the reforming reaction and $\alpha$ and $\beta$ the reaction order of $CH_4$ and $H_2O$. The expression and the data given by Lee are used even though the conditions within the fuel cell anode and fuel channel are different from the test conditions. The $H_2O$ partial pressure level and electric field which are present in the SOFC situation [10] may alter the reforming rate. Within the open literature, little else is available.

The volumetric reaction rate $r^S$ is computed by assuming the shift reaction to be at equilibrium:

$$K = \frac{X_{CO_2} X_{H_2}}{X_{CO} X_{H_2O}} \tag{16}$$

The conservation laws (1)-(4), the constitutive laws (5)-(9) and the source term expressions (12)-(14) yield the following system of (coupled) elliptic equations:

$$\begin{aligned}
\mathrm{div}\ (-\sigma \mathbf{grad}\,\Phi) &= 0 \text{ in } I, C, E \text{ and A} && (17)\\
\mathrm{div}\ (-\lambda \mathbf{grad}\ T) &= \sigma \mathbf{grad}\,\Phi \mathbf{grad}\,\Phi + Q_{chem} \text{ in I, C, E and A} && (18)\\
\mathrm{div}\ \left(\sum_{i\in\mathcal{G}} c_{p\,i} \mathbf{N}_i\, T - \lambda \mathbf{grad}\ T\right) &= Q_{chem} \text{ in } \mathrm{Ch_f} \text{ and } \mathrm{Ch_a} && (19)\\
\mathrm{div}\ \left(-cD_{O_2,mix} \frac{\mathbf{grad}\, X_{O_2}}{1 - X_{O_2}}\right) &= 0 \text{ in C} && (20)\\
\mathrm{div}\ (-cV_{\mathrm{Ch_a}} X_i) &= 0,\ \text{for } i = O_2, N_2 \text{ in } \mathrm{Ch_a} && (21)\\
\mathrm{div}\ \left(-cD_{i,mix} \mathbf{grad}\, X_i + X_i \sum_{j\in\mathcal{G}} \mathbf{N}_j\right) &= r_i,\ \text{for } i = H_2, H_2O, CO, CO_2 \text{ and } CH_4 \text{ in A} && (22)\\
\mathrm{div}\ (-cV_{\mathrm{Ch_f}} X_i) &= r_i,\ \text{for } i = H_2, H_2O, CO, CO_2, CH_4 \text{ in } \mathrm{Ch_f} && (23)
\end{aligned}$$

## 3.4 Interface conditions

Due to the surface electrochemical reactions, discontinuities of the potential and heat flux at the electrode-electrolyte interfaces exist. Also in the 3D model, the heat and mass transfer between the gas channel and the solid parts will be taken into account as interface conditions. Note that in the 2D model, these become boundary conditions, since the temperature and the concentrations in the channels are then data to the model.
Let us write the interface conditions on the various unknowns and associated fluxes.

### Temperature and heat flux

The temperature is continuous throughout the solid domain. We shall model the boundary layer which exists external to the channel walls by a heat transfert law of the form:

$$[\mathbf{q}.\mathbf{n}]_S = h\,(T_S - T_G) \tag{24}$$

where $[\mathbf{q}.\mathbf{n}]_S$ denotes the outward normal flux to the solid wall, $h$ is a heat transfer coefficient, $T_S$ is the temperature of the solid wall and $T_G$ is the temperature of the gas.

The heat flux is continuous everywhere except at the anode/electrolyte interface, where the electrochemical reaction generates a heat source term

$$[\mathbf{q}.\mathbf{n}]_E + [\mathbf{q}.\mathbf{n}]_A = \frac{[\mathbf{j}.\mathbf{n}]_A}{2F} T\Delta S \text{ at E/A} \tag{25}$$

where $\Delta S$ is the entropy of the reaction

$$\frac{1}{2}O_2 + H_2 \leftrightarrow H_2O \tag{26}$$

Note that this model does not take into account the effect of radiation. Work is under progress to include the radiation equations in the unit cell model [7]; these generate a 4th order nonlinearity which requires a specific numerical procedure.

**Species concentration and mass flux**

The species concentrations $X_i$ are studied in the channels and the porous electrodes. The conservation of the electrons must be written at the interfaces where the electrochemical reactions occur. Hence the mass flux is related to the electric current by Faraday's law:

$$[\mathbf{N}_{O_2}.\mathbf{n}]_C = \frac{[\mathbf{j}.\mathbf{n}]_E}{4F} \text{ at C/E,} \tag{27}$$

$$[\mathbf{N}_{H_2}.\mathbf{n}]_A = \frac{[\mathbf{j}.\mathbf{n}]_A}{2F} \text{ at E/A.} \tag{28}$$

**Potential and electric current**

The potential is continuous throughout the solid parts except at the electrode/electrolyte interfaces where the electrochemical reactions occur. These potential jumps are modelled by Nernst's law and write

$$\Phi_C - \Phi_E = \frac{\mathrm{R}T}{4\mathrm{F}}\ln(X_{O_2}) - R_{O_2}[\mathbf{j}.\mathbf{n}]_E \tag{29}$$

$$\Phi_E - \Phi_A = -\frac{\Delta G}{2F} - \frac{\mathrm{R}T}{2\mathrm{F}}\ln\left(\frac{X_{H_2O}}{X_{H_2}}\right) - R_{H_2}[\mathbf{j}.\mathbf{n}]_A \tag{30}$$

where $\Delta G$ is the Gibbs free energy change of the reaction (26), $R_{O_2}$ and $R_{H_2}$ are the polarisation resistivities.
The electric current is continuous everywhere in the solid part, and is linked to the mass flux at the electrode-electrolyte interfaces by Faraday's law (27)-28).

At the channel/solid interface, the electric current is of course null, hence the condition

$$\sigma \mathbf{grad}\,\Phi.\mathbf{n} = 0 \text{ on } \Gamma_{\mathrm{Ch_a}} \text{ and } \Gamma_{\mathrm{Ch_f}} \tag{31}$$

## 3.5 External boundary conditions

The boundary conditions on $\Phi$, $T$ and $X_i$ (and/or on the associate fluxes) on the external boundary of the cell remain to state be stated. These boundary conditions depend on the operating conditions. The boundary conditions considered here are based on the idea that the cell is part of a whole stack and that the overall behaviour is periodic. So on the lateral boundary $\Gamma_L$ we state that :

$$[\mathbf{j}.\mathbf{n}]_{\Gamma_L} = 0 \tag{32}$$

$$[\mathbf{q}.\mathbf{n}]_{\Gamma_L} = 0 \tag{33}$$

$$[\mathbf{N}_i.\mathbf{n}]_{\Gamma_L} = 0 \tag{34}$$

$$\text{for } i = O_2, H_2, H_2O, CO, CO_2, CH_4$$

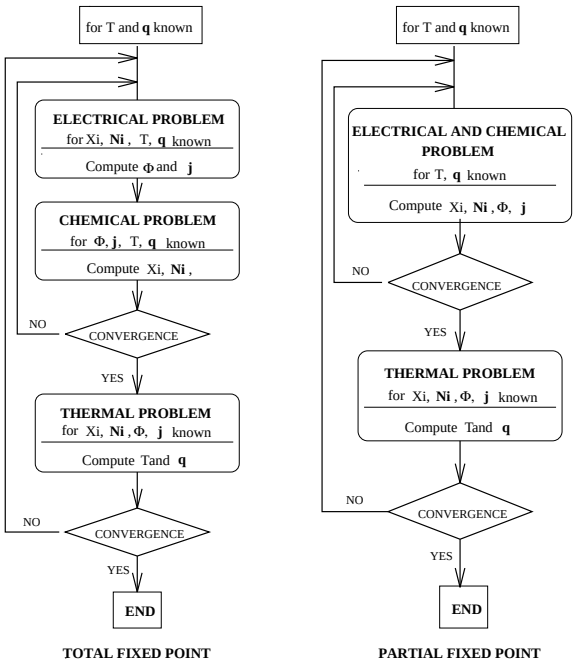


Figure 6: Solution procedure

Periodicity conditions are imposed for the temperature on the top and the bottom of the cell whereas a mean current value $\mathbf{j}_{avg}$ is imposed for the current, i.e. :

$$[T]_{\Gamma_T} = [T]_{\Gamma_B} \tag{35}$$

$$[\mathbf{q}.\mathbf{n}]_{\Gamma_T} = -[\mathbf{q}.\mathbf{n}]_{\Gamma_B} \tag{36}$$

$$[\mathbf{j}.\mathbf{n}]_{\Gamma_T} = -[\mathbf{j}.\mathbf{n}]_{\Gamma_B} \tag{37}$$

$$[\mathbf{j}.\mathbf{n}]_{\Gamma_T} = \mathbf{j}_{avg} \tag{38}$$

Finally the temperature, the molar fractions and the molar flux are imposed at the inlet face of the gas channels.

# 4 Numerical implementation

## The numerical procedure

The necessary step in order to perform a numerical simulation is to discretize the set of equations in $T$, $\Phi$ and $X_i$. The equations themselves are of the Laplace type in the solid part and can be successfully discretized by any of the usual methods, i.e. finite differences, finite element or finite volumes. However, a finite volume discretization (see [27], [12] for an introduction) was preferred over the finite element method because it is computationally cheaper for the problem at hand, as can be seen from the results shown in [17]. Moreover, an advantage of the finite volume method is that it is "close to the physics" in the sense that it is based on writing the balance of the fluxes through the boundaries of a discretization cell (which is called a "control volume"), and therefore all source terms can be accounted for in a natural way. The discretization of the equations yields a nonlinear finite system, where the unknowns are the average values (over the control volumes) of $T$, $\Phi$ and $X_i$.
The equations in $T$, $\Phi$, $X_i$ are coupled by the electric conductivity (which depends on the temperature), the ohmic source terms and the interface source terms, both in $T$ and $\Phi$. A rather straightforward iterative method is used, which computes, for a given temperature, the solution to the mass and electric problems ($X_i$ and $\Phi$), and once convergence is obtained, solves the temperature problem.

| Gas | Temp. | $O_2$ | $N_2$ | $H_2$ | $H_2O$ | $CO$ | $CO_2$ | $CH_4$ |
|---|---|---|---|---|---|---|---|---|
| Air | 1173 K | 21 % | 79 % | | | | | |
| Fuel I | 1173 K | | | 90 % | 10 % | | | |
| Fuel II | 1173 K | | | 26.26 % | 49.34 % | 2.94 % | 4.36 % | 17.10 % |

Table 1: Gas temperature and composition at inlet

| | | | | |
|---|---|---|---|---|
| Average current density | $300\,mA/cm^2$ | | | |
| Fuel utilization | 85 % | | | |
| Air ratio | 7 | | | |
| Pressure | 1 bar | | | |
| Over potential | cf. [28] | | | |
| Electrical $\sigma$ $(\Omega^{-1}m^{-1})$ and thermal $\lambda$ $(Wm^{-1}K^{-1})$ conductivities | | | | |
| | Cathode | Electrolyte | Anode | Interconnect |
| $\sigma$ | $\frac{4.2\,10^7}{T}exp-\frac{1200}{T}$ | $3.34\,10^4 exp-\frac{10300}{T}$ | $\frac{9.5\,10^7}{T}exp-\frac{1150}{T}$ | $\frac{9.3\,10^6}{T}exp-\frac{1100}{T}$ |
| $\lambda$ | 50% | – | 50 % | – |
| $\lambda$ | 3 | 2 | 3 | 3.5 |
| Diffusion coefficient | $D_{O_2}$ | $D_{H_2}$ | $D_i$ (Fuel II) | |
| Values $(cm^2s^{-1})$ | $0.181 * \left(\frac{T}{273}\right)^{1.5}$ | $0.753 * \left(\frac{T}{273}\right)^{1.5}$ | $0.364 * \left(\frac{T}{273}\right)^{1.5}$ | |

Table 2: General operating conditions

## The computer code

The computer program, called SOFC3D, consists of two parts. The first part is the computational kernel and database manager. It was written using the C language and contains 11000 instructions. It has been used on several UNIX systems, e.g. Silicon Graphics, SUN, CRAY. The database input file contains the parameters which define the geometries (planar, cylindrical or tubular), the composition of the fuel (hydrogen or methane), the computational mesh and the set of operating conditions. (Currently, a user-friendly graphic X interface is being developped [6].) The second part is a 10000 lines graphic software which includes a user-friendly mesh generator and a 3D-graphics post-processor.

The results which are presented here were obtained on a INDIGO SG work-station with a 50MHz R4000 processor and 32 MB of real memory. The database file requires about 100 MB of disk memory.

## Validation of the numerical code

Since we have no experimental data to compare to, we validate our code by comparing the results obtained for a benchmark which was defined by participants of the IEA program for the numerical simulation of a planar geometry with 18 fuel and air channels. Note that, throughout these tests, in accordance with the IEA benchmark, the porosity is not taken into account and the thermal conductivity is constant and equal to 2 $Wm^{-1}K^{-1}$. Here, as in [2], the overpotential at each interface is set to the ohmic loss of the electrolyte. Results are given in Table 3 (results from IEA were taken from [2]). It appears that in most of the models cited in Table 3, the diffusion effect of the gaseous species in the electrodes is only accounted for in the direction orthogonal to the channel axis. We implemented both this "1D diffusion" and the three dimensional diffusion effect. Hence, two series of results from our code are listed in table 3, labeled "1D diff" and "3D diff". The "3D diff" cell voltage computed with our code is somewhat smaller than the average cell voltage. However, the "1D diff" cell voltage which we compute is closer to the voltages obtained by the other models. We show in the next section that when the 3D effect is accounted for, the concentration profile at the electrode/electrolyte interface is not constant and that the low values of concentrations underneath the rib decreases the efficiency of the cell. The effect of the decrease of activity underneath the rib is recognised to be also of importance in stack modelling [21], it is therefore worthwhile trying to measure it quantitatively

| | *Cell voltage* | | *Max solid temp* | | *Min solid temp* | |
|---|---|---|---|---|---|---|
| Author | counter | co | counter | co | counter | co |
| Dornier (D) | 0.689 | 0.684 | 1085 | 1070 | 914 | 928 |
| ECN Petten (NL) | — | 0.704 | — | 1082 | — | 899 |
| Eniricerche (I) | 0.730 | 0.722 | 1083 | 1069 | 906 | 916 |
| Inst. for energiteknikk (N) | 0.71 | 0.71 | 1084 | 1058 | 912 | 930 |
| KFA-Jülich (D) | 0.712 | 0.706 | 1073 | 1059 | 906 | 913 |
| Siemens (D) | 0.716 | 0.712 | 1062 | 1049 | 904 | 909 |
| Statoil (N) | 0.709 | 0.702 | 1082 | 1098 | 913 | 970 |
| RisØ (DK) | 0.7101 | 0.7034 | 1075 | 1061 | 910 | 924 |
| SOFC3D (3D diff.) | 0.7080 | 0.6955 | 1055 | 1037 | 920 | 921 |
| SOFC3D (1D diff.) | 0.7203 | 0.7079 | 1054 | 1036 | 920 | 918 |

Table 3: Comparison with the IEA benchmark

at the cell level.

The code can simulate a cell using pure hydrogen only, or using methane with internal reforming. Tables 1 and 2 gives the general operating parameters for both cases. These parameters will be used throughout the numerical runs, unless otherwise mentionned. The following section is devoted to the numerical results which are obtained by running the code on different geometries of adiabatic cells, and the use of these results for cell optimization.

# 5 Using the code as a design tool

## Comparison of the co-, counter- and cross- flow cases

Numerical tests were performed in the case of the co- and counter-flow for a planar geometry of a 10 cm long unit cell with the following parameters: active area 5.42x100 $mm^2$, anode thickness 50 $\mu m$, cathode thickness 50 $\mu m$, electrolyte thickness 150 $\mu m$, channel width 3mm, channel height 1mm, rib width 2.42 mm, total bipolar plate thickness 2.5 mm.

Figure 7 gives a comparison of the efficiency (i.e. the ratio of electrical energy to chemical energy at inlet) of geometry with 5 fuel and air channels for the co-, counter- and cross- flow designs, as a function of current density. In this numerical test, the porosity is not taken into account and the thermal conductivity is constant and equal to 2 $Wm^{-1}K^{-1}$ as in the IEA experiments. The overpotential used is defined in [2].

These computations show the counter flow design as being most efficient. Note that this is in agreement with the results given by the different models of the IEA (see table 3) but it contradicts the results of [14], where only the 1D effects were taken into account. The superiority of the counter flow geometry was also found by numerical experiments on a 3D stack [1] including the reforming effect. This better performance can be explained by the fact that the temperature distribution is then better for the efficiency of the reforming reaction.

## Influence of rib width on overall efficiency

The conducting material between two channels is generally called the rib. The rib width seems to be an important parameter for the efficiency of the cell:

- on one hand, the wider the rib, the smoother the electrical current. Hence a wider rib will give a better conduction of the electrical current and less ohmic losses.
- on the other hand, the wider the rib, the narrower the channel; when the channel width decreases, the chemical species do not diffuse as well underneath the rib.

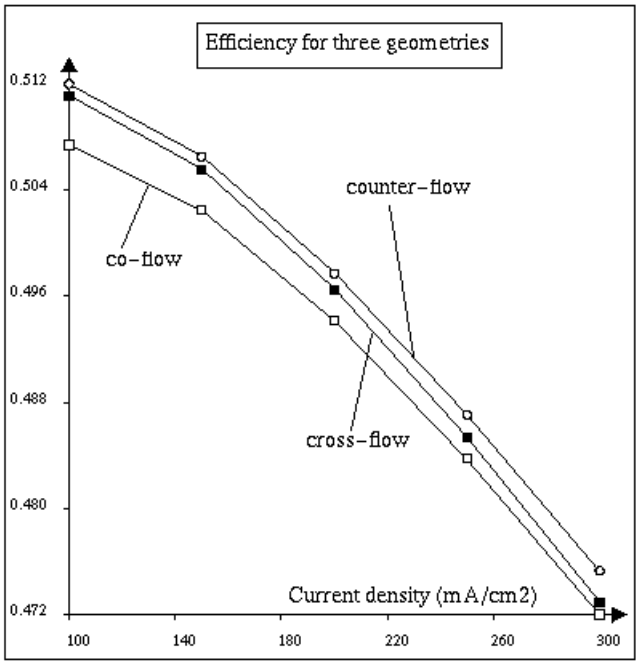


Figure 7: Efficiency of co-, counter- and cross- flow geometries

Therefore the numerical code can be used to check if an optimal value can be obtained for the rib width. The numerical results confirm the competing effects: when the rib width increase (with all other parameters fixed), the ohmic loss decreases (Figure 8), but the potential jump also decreases (Figure 9). With all other parameters set to the values indicated in tables 1 and 2, an optimal rib width of 2.2 mm is obtained, as indicated on Fig. 10.

## Influence of electrode thickness on efficiency

We study here the influence of the electrode thickness on the concentration of $H_2$ at the anode/electrolyte interface and on the concentration of $O_2$ at the cathode/electrolyte interface. It is clear that a thicker interface electrode will be more resistant to the diffusion of the gaseous species; in order to study the significance of this effect we use the 2D pure hydrogen model for a co-flow geometry. We found that the cell voltage which we obtained with our initial model (labeled "3D diff") could be significantly increased if the diffusion of the gas in the porous medium was taken to be only in the direction normal to the electrolyte/anode interface (which is the case in most models and in our simplified model labeled "1D diff"). In our model, however, the diffusion effect is accounted for in all directions, and the hydrogen concentration at the electrode/electrolyte interface is much lower away from the channel than close to it. This is clearly seen on Figure 11, which represents the hydrogen concentration profile for various anode thicknesses, using pure hydrogen as a fuel.

Figure 5 represents the PEN potential jump computed with the Nernst law w.r.t. the molar fractions in the channels, at the interface electrode/electrolyte, and with the maximum value of the molar fraction at the electrode/electrolyte interfaces. Taking this last value is in fact assuming a 1D diffusion in the porous electrode. It is clear from Figure 5 that the 3D effect in the diffusion loss is quite important, and that it can in fact become dramatic in the case of a narrow anode.

In the case where methane is used, above results will be altered since the methane reforming rate increases with the anode thickness (and the amount of the catalyst), assuming a volumetric reforming reaction. There are now several competing effects which play a role in the optimization of the anode thickness:

Figure 8: Ohmic loss vs rib width

Figure 9: PEN potential jump vs rib width

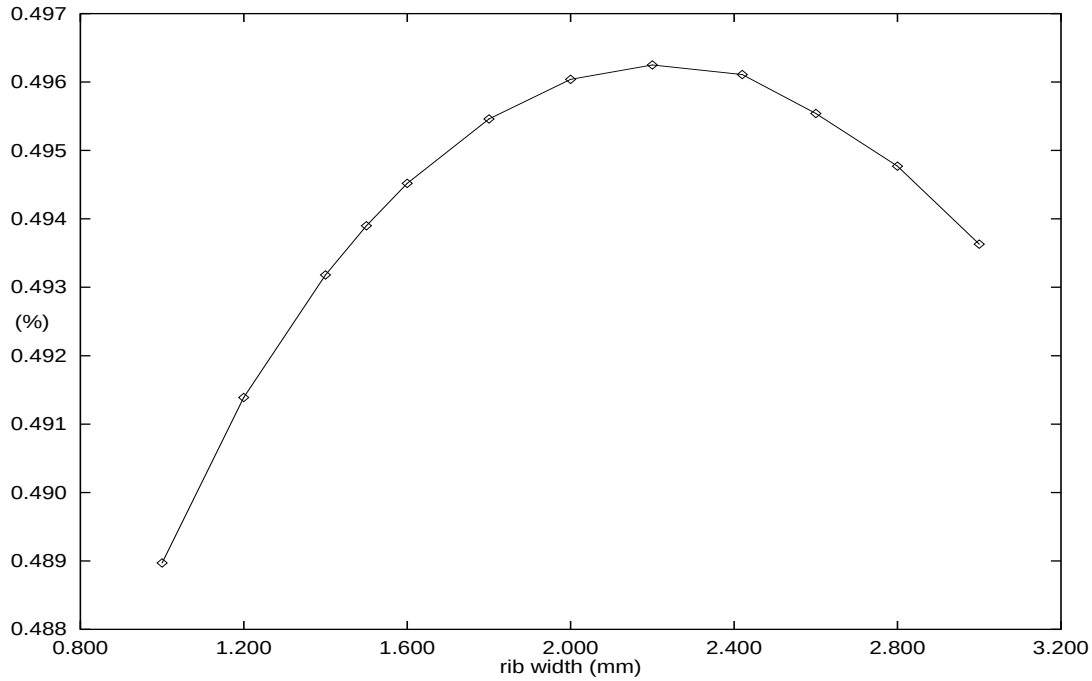


Figure 10: Efficiency vs rib width, pure $H_2$ model

Figure 11: $H_2$ molar fraction profile, anode thickness 100, 200, 800 $\mu m$

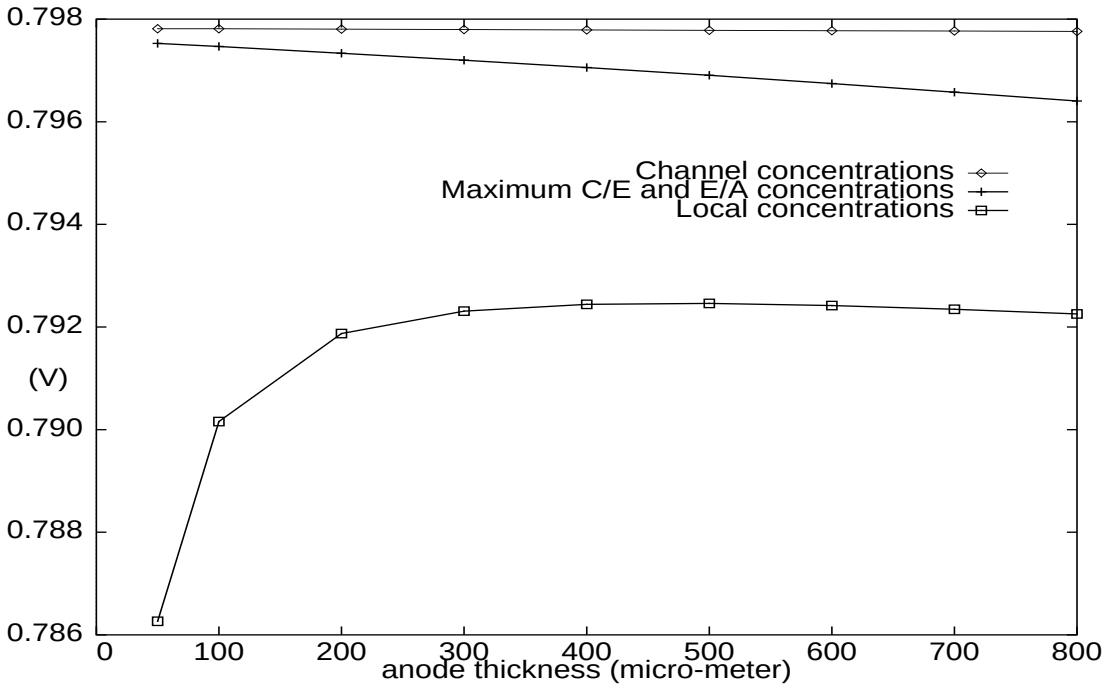


Figure 12: PEN potential jump vs anode thickness

- the diffusion of gas is better for a relatively thin anode (but not too thin, as observed in Figure 5),
- the production of methane by volumetric reforming increases with the thickness of the anode (see Figure 13);
- the methane reforming is an endothermic reaction, so that when the methane production increases, it decreases the temperature;
- the ohmic loss increases with the anode thickness, which tends to increase the temperature.

The numerical code simulating the 3D model for methane in the planar geometry was used to study this phenomenon. The input parameters were set as in Table 1 and 2, with a fixed inlet fuel flux($= 0.0385\, mol/h$). The thickness of the anode was varied from $50\,\mu m$ to $800\,\mu m$. In fact for a anode thickness of $50\,\mu m$, there is not enough hydrogen produced by reforming for the requested produced current, and the numerical code cannot reach a solution.
The results (figure 14) show that for a planar geometry, a thickness of $200\,\mu m$ seems to be optimal with respect to the efficiency (defined as the ratio of the electric power over the chemical power of the inlet gas). It can be observed from Figure 15 that the Nernst potential increases steadily with the anode thickness, but so do the ohmic losses (figure 16) and the polarization losses (figure 17). Note that the fuel utilzation decreases wtih the anode thickness (figure 18).
The minimal temperature may go below the inlet temperature of the fuel because of the endothermic characteristic of the reforming reaction, as may be seen in Figure 19. This is in agreement with the remarks on a "cold cell" of [22]. The rib effect may again be seen on Figure 20.

## Results for other geometries

The adaptivity of our 3D SOFC code can be demonstrated by running numerical simulations on other fundamental geometries. Here a sample of results concerning a tubular (Westinghouse concept) geometry and a cylindrical geometry are given.

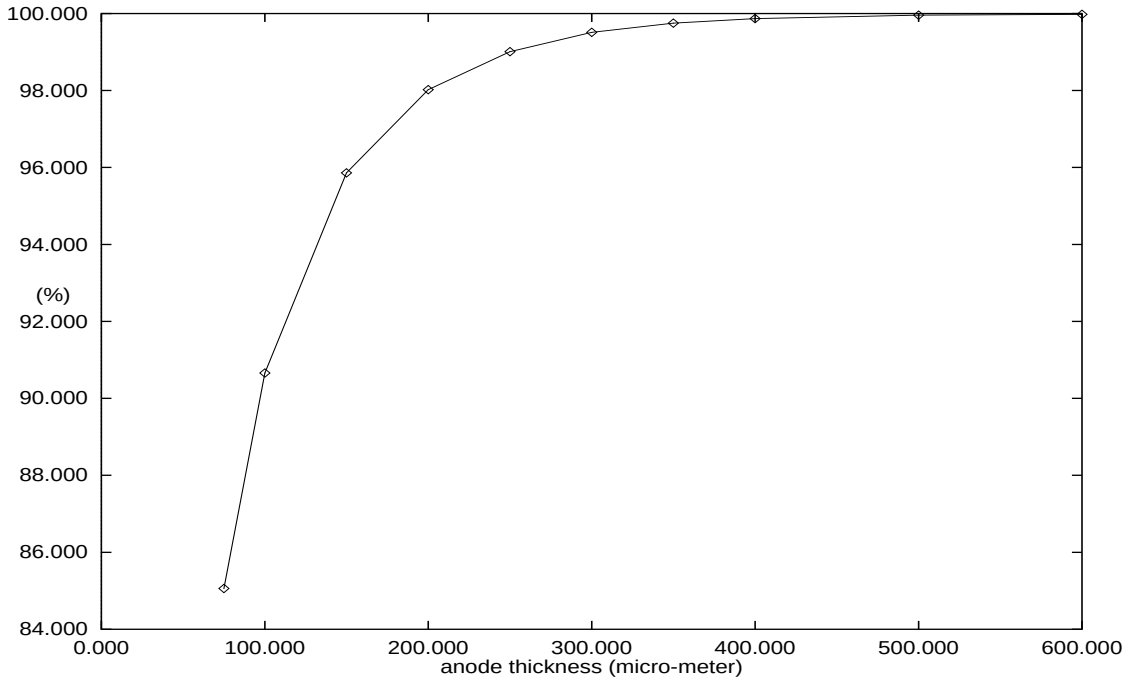


Figure 13: Methane conversion vs anode thickness

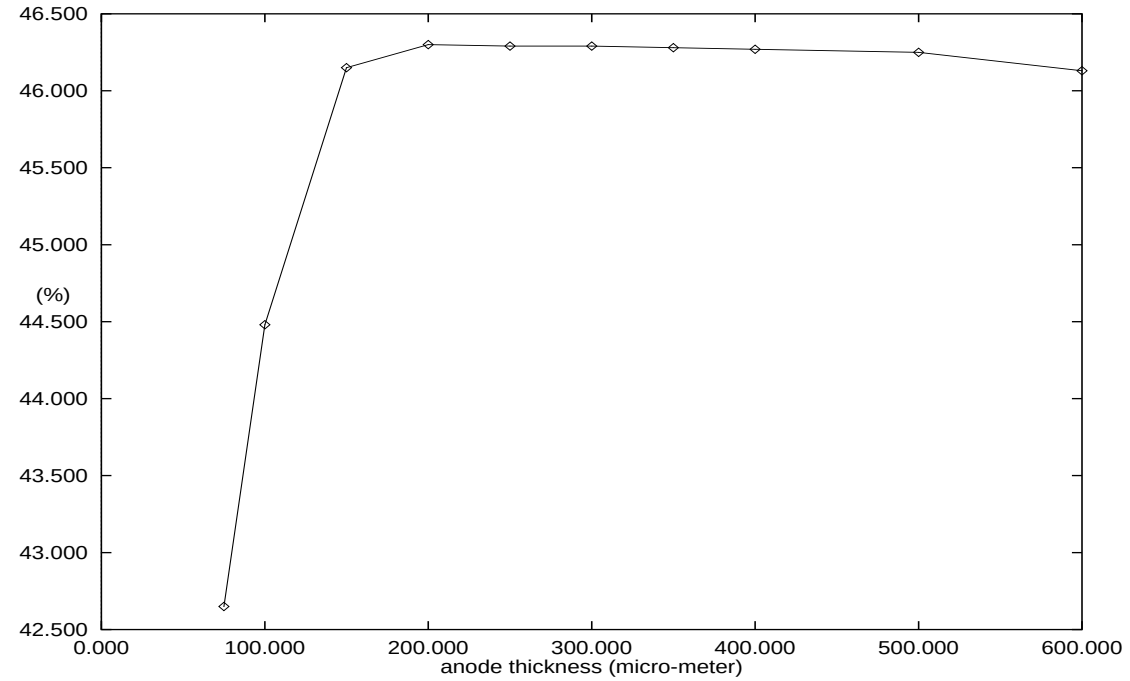


Figure 14: Efficiency vs anode thickness

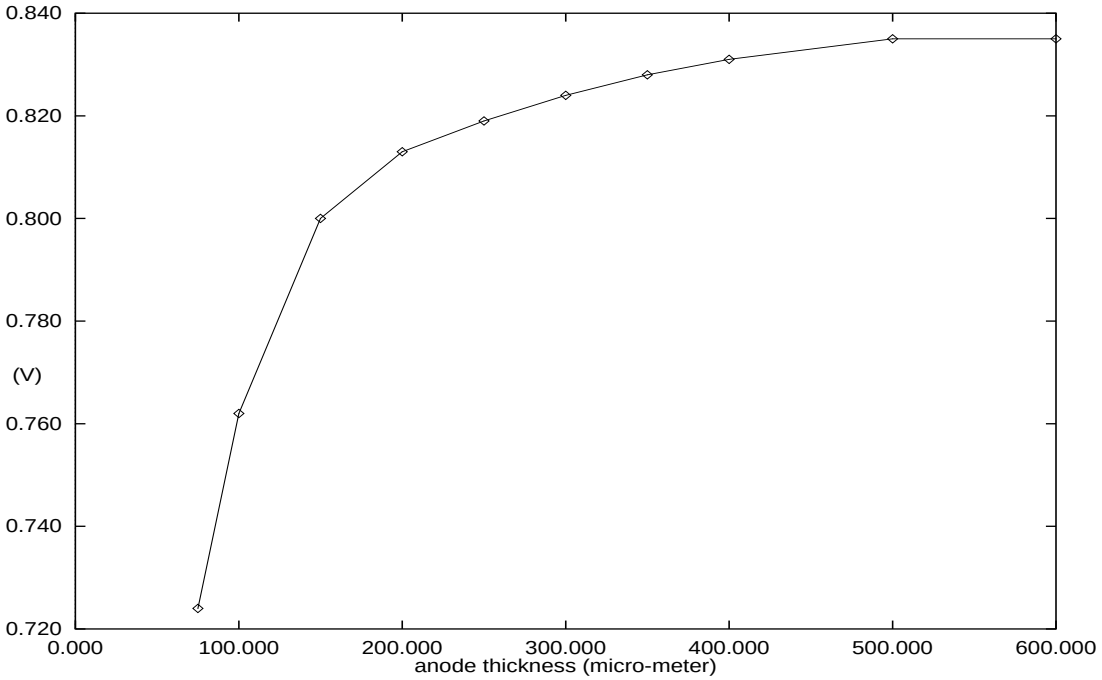


Figure 15: Nernst potential at the electrolyte level vs anode thickness

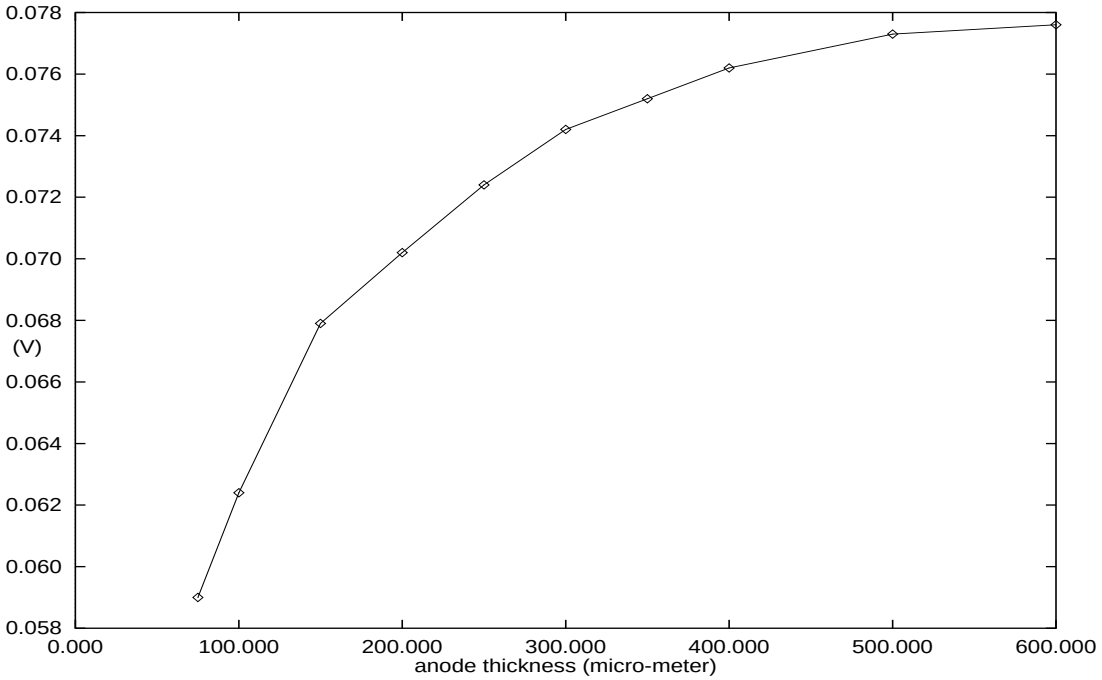


Figure 16: Ohmic losses vs anode thickness

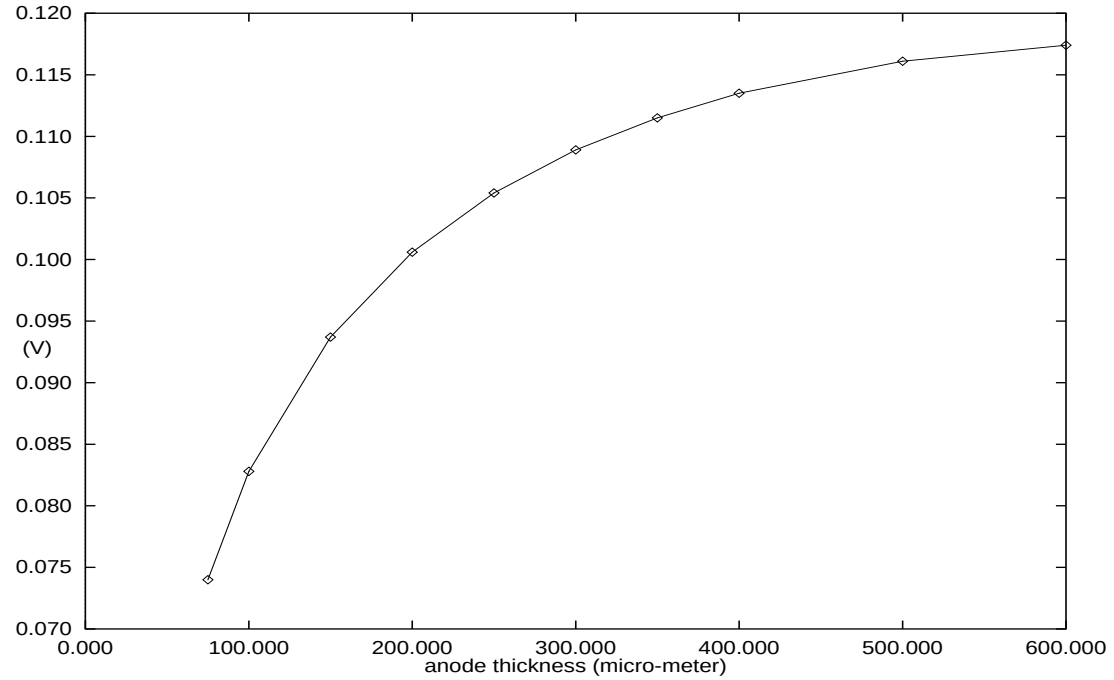


Figure 17: Polarisation Losses vs anode thickness

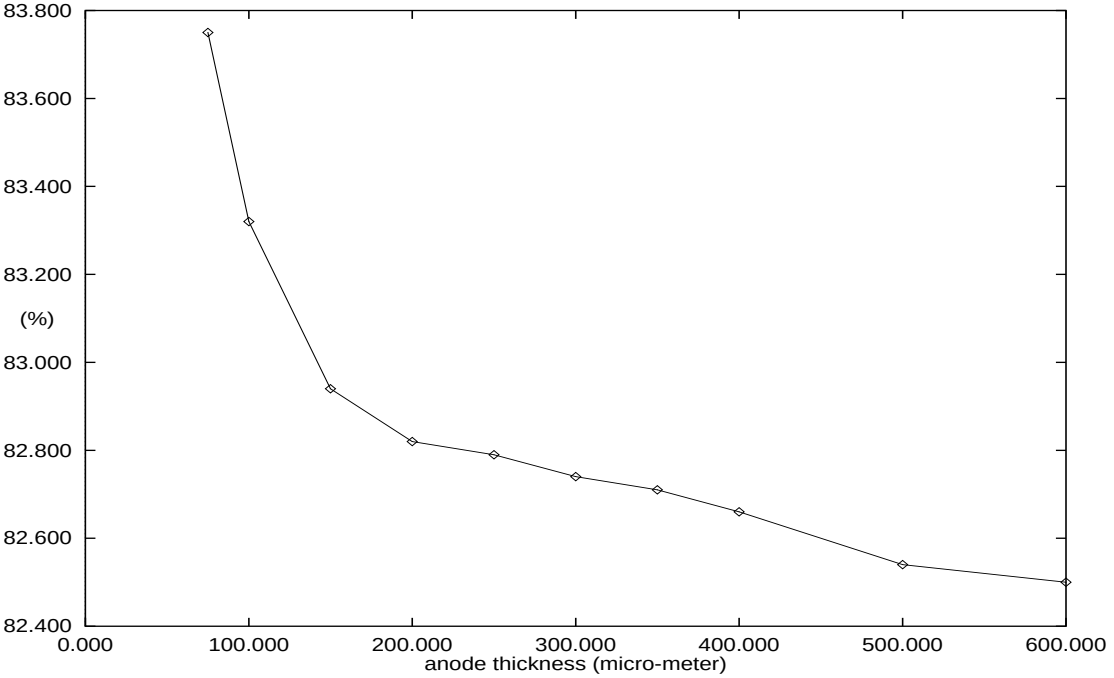


Figure 18: Fuel utilization

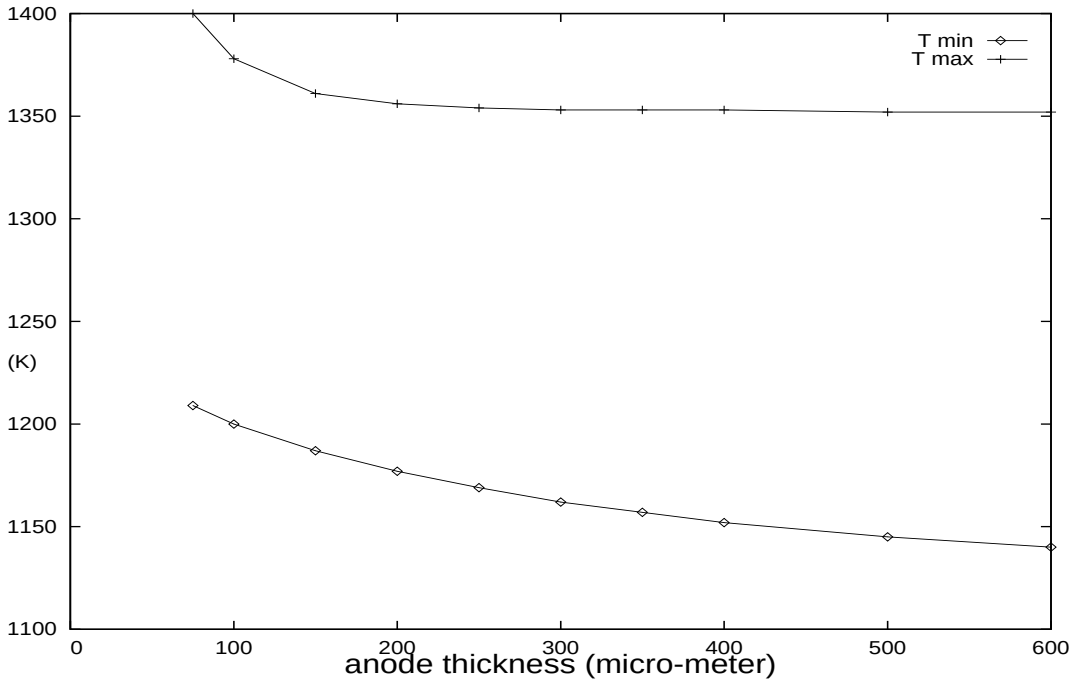


Figure 19: Maximum and minimum temperatures vs anode thickness

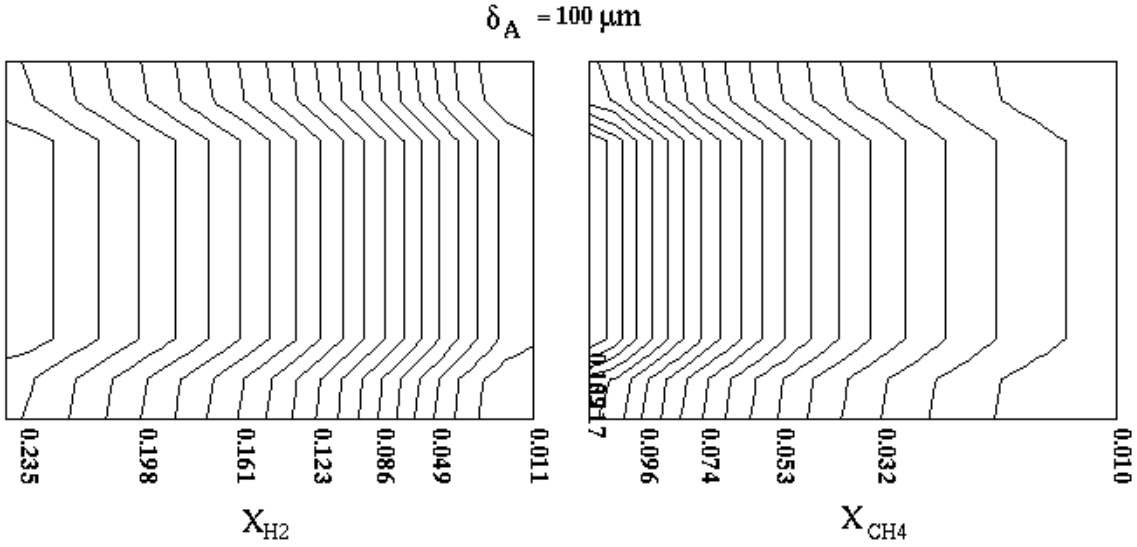


Figure 20: $H_2$ and $CH_4$ molar fraction on a section parallel to the gaz channel

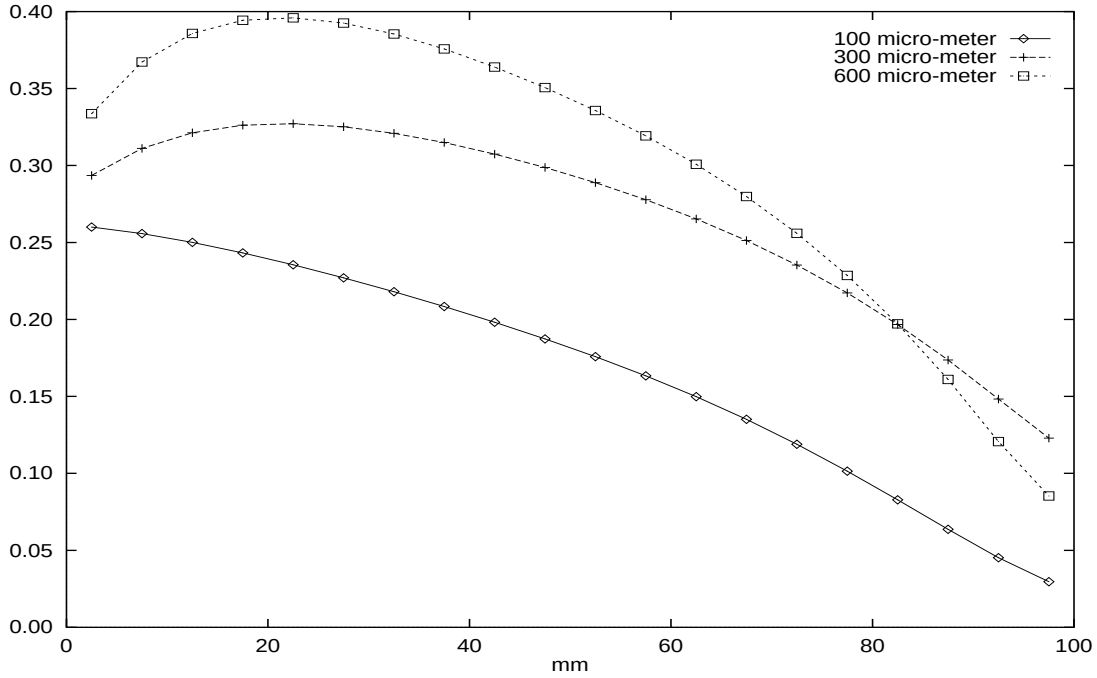


Figure 21: $H_2$ molar fraction at the center point of the anode cross-section for several anode thicknesses (100, 300, 600 micro-meter)

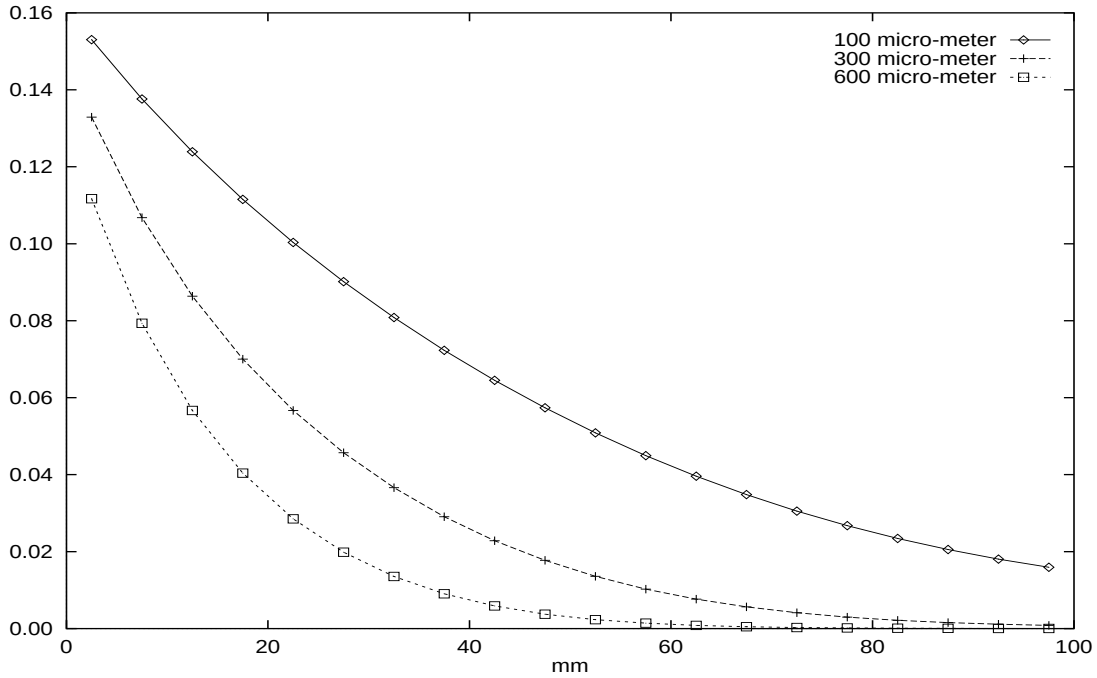


Figure 22: $CH_4$ molar fraction at the center point of the anode cross-section for several anode thicknesses (100, 300, 600 micro-meter)

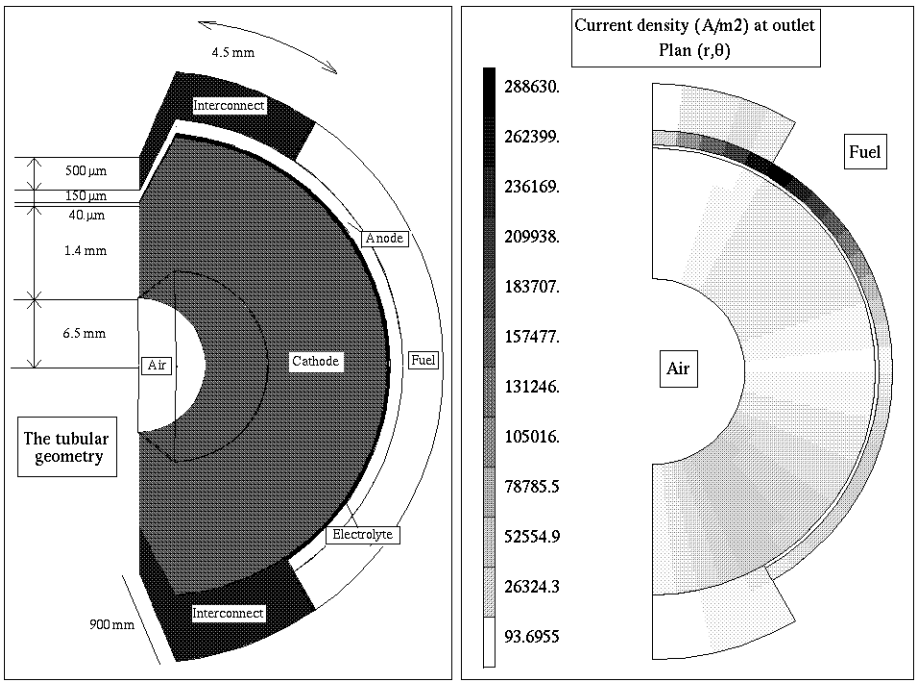


Figure 23: 3D section of the tubular design and current density at outlet section

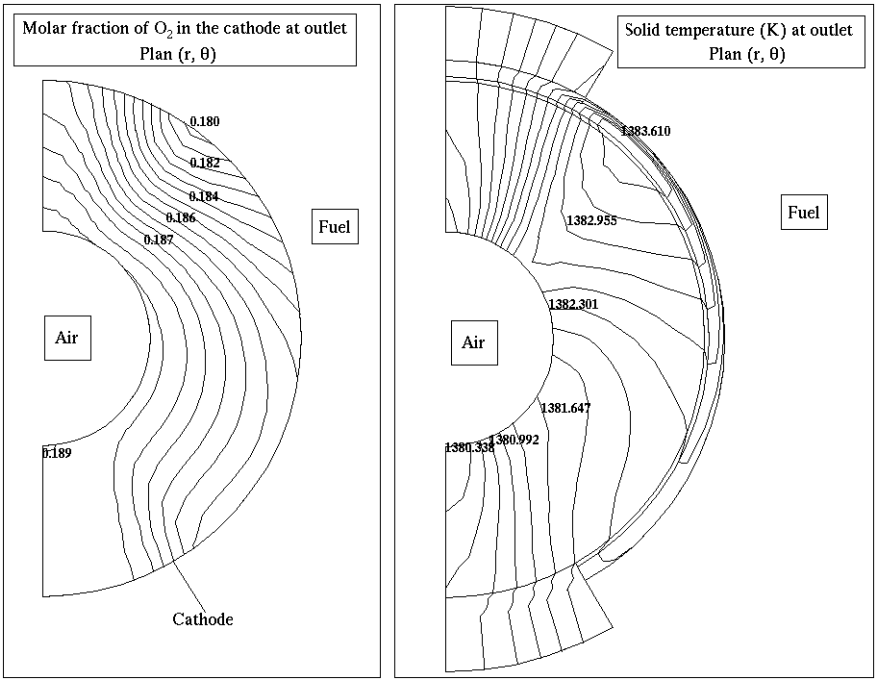


Figure 24: Molar fraction of $O_2$ and temperature at outlet section

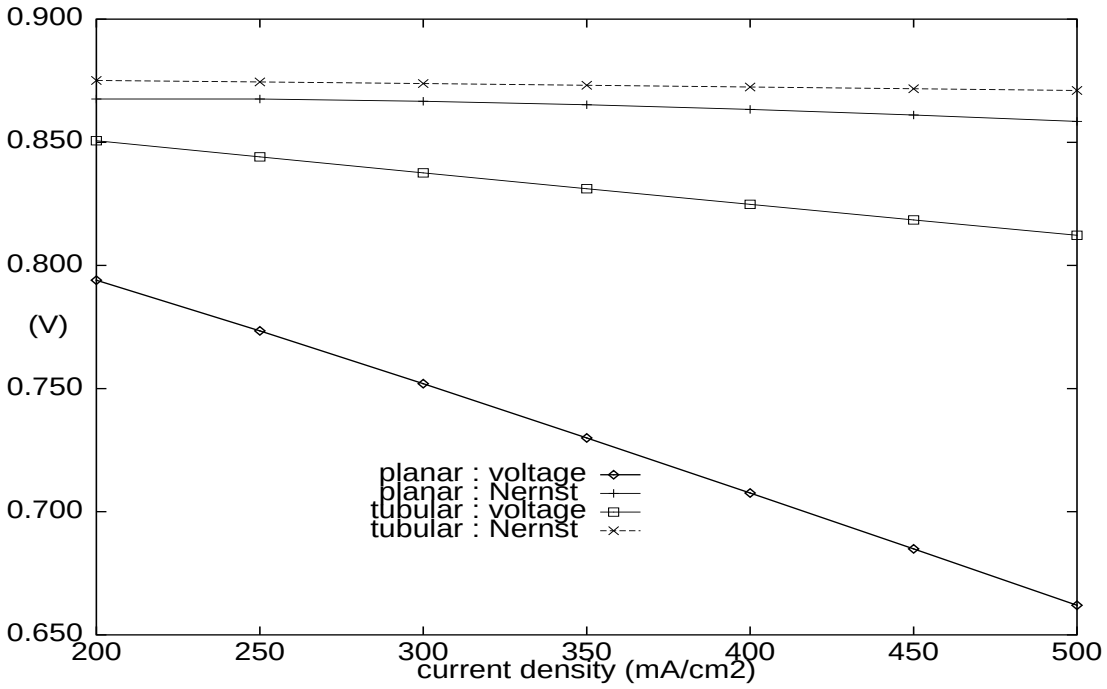


Figure 25: Comparison of the tubular and planar geometries

**The tubular geometry**

In this test, the mean current density is taken equal to 1500 $mA/cm^2$ in the interconnect. The dimensions of the cell were taken from [11] and [18] and are shown in Figures 23. Figure 23 also shows the contours of current density at the outlet section of the cell. It can be noted that the highest density is near the interconnect/anode interface; this is due to the fact that the anode is thin, and that the interconnect area is not very large. On the cathode side, however, the current density is lower because the cathode is thicker. Figure 3 shows the contours of the molar fraction of oxygen and the temperature at the oulet section of the cells. Note that the minimum of the molar fraction of $O_2$ and the maximum temperature are reached in the region of highest current density. Figure 25 shows the comparison of the potential drops for a planar geometry and a tubular geometry which were chosen such that the input electric current are the same on the upper surface of both geometries. These results show that the tubular geometry is more efficient.

**The cylindrical geometry**

In the absence of data for a so-called "cylindrical" geometry, we derived the dimensions of a cylindrical cell by distorting a planar cell. The dimensions of the cell are shown on Figure 26. The computations were performed on a "slice" of the cell only, taking symmetry considerations into account. The mean current density is taken equal to 180 $mA/cm^2$. Figure 27 shows the distribution of temperature in the electrolyte and Figure 28 the distribution of hydrogen in the anode. Again, one can see that the diffusion is always weaker at the center of the rib.

# 6 Conclusion

A 3D numerical code was developped for the numerical simulation of solid oxide fuel cells and stacks, which can be used for various geometries of SOFC's. The mathematical model is based on a local balance approach, and the finite volume method was found to be well adapted for our problem. Numerical runs were performed first to validate our code with a benchmark which was defined py the participants to IEA; the results which

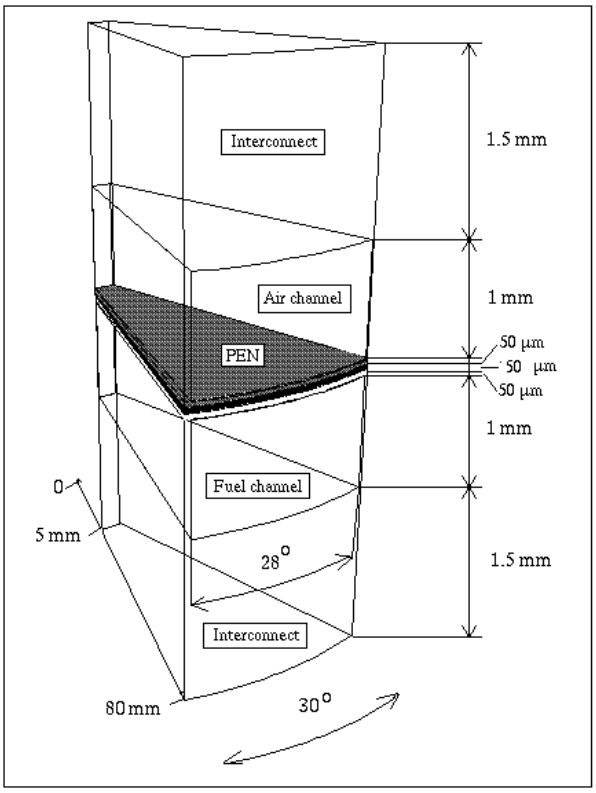


Figure 26: Geometry of a cylindrical cell

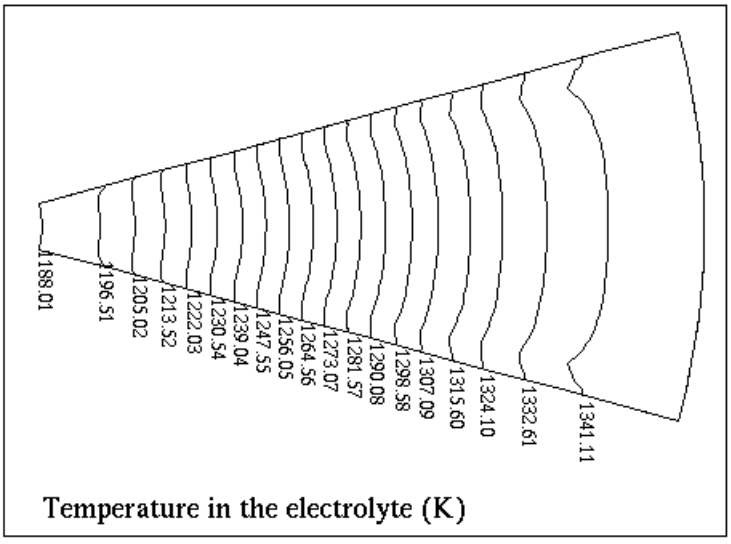


Figure 27: Temperature distribution in the electrolyte

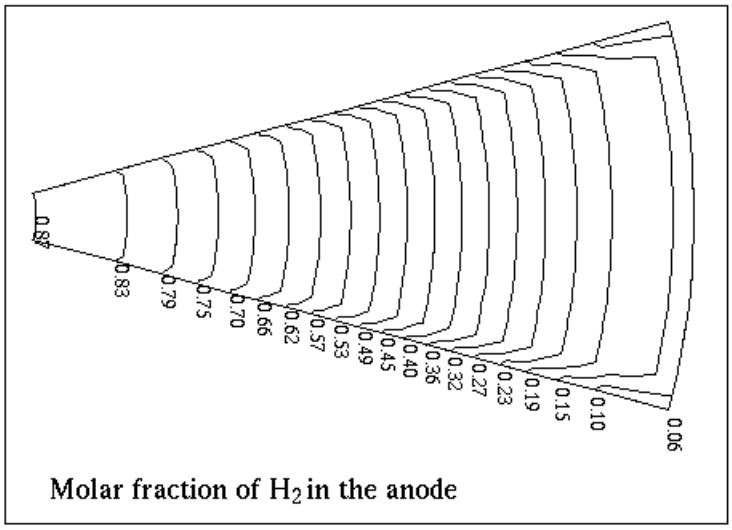


Figure 28: Molar fractions in the anode

were obtained with our code were pretty much in agreement wih those of IEA for the test case (with hydrogen as a fuel), except for the fact that our code seemed to be a little more pessimistic than most others with respect to the electrical potential of the cell. This is probably due to diffusion effect which our model takes into account more accurately. The code was then used as a design tool for the cell geometry: we compared the cross, counter and co-flow designs for a planar geometry and found that the counter flow was optimal (with hydrogen as a fuel). We also found that we could use the code to compute the optimal value of one given parameter, such a the rib width, or the anode thickness. In the latter case, the reforming effect was studied (using methane as a fuel). Comparisons between the tubular and the planar geometry were carried out, and showed less ohmic loss for the first geometry. The flexibility of our code allows the simulation of several geometries. Indeed, a new geometry could be introduced relatively easily thanks to the modularity of the code.

Further work includes the study of the effect of the radiation inside the fuel and air channels. In [22], the effect of radiation was introduced at the stack level by means of the computation of an "effective thermal conductivity" [22], and it was shown in [19], using a finite element approach for temperature and electrical current that the radiation effect has a definite influence on the temperature distribution. A sensitivity analysis with respect to the geometry parameters, w.r.t. the physical properties of the constitutive materials and w.r.t. the operating conditions is also planned.

**Aknowledgement**: This work was supported by Gaz de France and ADEME (Agence de l'Environnement et de la Maîtrise de l'Energie)

# References

[1] E. Achenbach Three dimensional and time-dependent simulation of a planar solide oxide fuel cell stack, *J. Power sources, 49, 338-348, 1994.*

[2] E. Achenbach with KFA-IER, Status of the IEA-Bench Mark Test 1 on Stack-Modelling. *IEA-Workshop, Rome 22-23 Avril 1994*

[3] E. Achenbach, Simulation of SOFC System Dynamics, *Proc. First European Solid Oxid Fuel Cells Forum, U. Bossel Ed., Luzern, Switzerland, 1994.*

[4] A.J. Appleby & F.R. Foulkes, Fuel Cell Handbook, *Van Nostrand Reinhold, New York, 1989.*

[5] Ph. Batoux, Homogeneisation of linear elliptic operators on an ope set with holes, *submitted.*

[6] M. Bernier, Maintenance et développement d'un simulateur de pile au gaz naturel, *Université de Savoie, 1994.*

[7] M. Bernier & R. Herbin, Numerical solution to a heat transfer problem with radiation boundary conditions, *in preparation.*

[8] R.B. Bird, W.E. Steward & E.N. Lightfoot, Transport Phenomena, *John Wiley and Sons, New York, 1960.*

[9] U.G. Bossel & J.R. Ferguson, Natural Gas Fuelled Solid Oxide Fuel Cells and Systems, Facts and Figures, *International Energy Agency Workshop, Charmey, Switzerland, 1989.*

[10] P.G. Debenedetti & C.G. Vayenas, *Chem. Eng. Sci.,38, 11, 1817-1823, 1983.*

[11] Draper, Solid oxide fuel cell generator, *United States Patent, Avril 1994*

[12] R. Eymard, T. Gallouët & R. Herbin, The finite volume method, *in preparation for Handbook of Numerical Analysis, Ph. Ciarlet and J.L. Lions eds, North-Holland.*

[13] J.R. Ferguson, SOFC Modelling, *2nd OFEN Report,1991, Berne, Suisse.*

[14] J.R. Ferguson, Analysis of Temperature and Current Distributions in Planar SOFC Designs, *2nd International Symposium on Solid Oxide Fuel Cells, Juillet 2-5,1991, Athens, Greece.*

[15] J.R. Ferguson, J.M. Fiard et R. Herbin, A two-dimensionnal simulation of a solid oxide fuel cell, *IEA Workshop : Fundamental Barriers to SOFC performance, Lausanne, Suisse, Août 1992, publié par OFEN, CH-3003, Berne, Suisse.*

[16] J.M. Fiard & R. Herbin, Numerical simulation of solid oxide fuel cells at the cell and stack level, *Eurogas92, Trondheim,June 1992, published by NTH-SINTEF, Norway.*

[17] J.M. Fiard & R. Herbin, Comparison Between Finite Volume and Finite Element Methods For An Elliptic System Arising In Chemistry, *Comput. Methods Appl. Mech. Engrg. 115, 1994. 315-338.*

[18] C.A. Forges & J.F. Pierre, The solid fuel cell future, *IEEE Spectrum, Oct. 93, 40-44.*

[19] J. Hartvigsen, S. Elangovan & A. Khandkar, Modeling design and performance of Solid Oxide Fuel Cells, *Science and Technology of Zirconia V, Technomic, S.P.S. Badwal, M.J. Bannister & R.H.J. Hannink eds., 1993.*

[20] R. Herbin, J.M. Fiard & J.R. Ferguson, Three-Dimensional Numerical Simulation of the Temperature, Potential and Concentration Distributions of a Unit Cell for Various Geometries of SOFCs, *European Solid Oxide Fuel Cell Forum, Luzern, Switzerland, 1994.*

[21] H. Karoliussen, K. Nisancioglu & R. Ødegård, The role of certain design and operating parameters on SOFC stack performance, *IEA Advanced Solid Oxide Fuel Cells, 6th Workshop and experts meeting, Rome, 1994.*

[22] H. Karoliussen, K. Nisancioglu, A. Solheim & R. Ødegård, SOFC stack modelling with reforming, *Proc. 3Rd Int. Symp. on SOFC, Honolulu, Hawaii, The Electrochemical Society, Pennington, 1993.*

[23] A.L. Lee, Internal Reforming Development for Solid Oxide Fuel Cells, *DOE/MC/ 22045-2364 report from Institute of Gas Technology, 1987.*

[24] A. Malandrino & M. Chindemi, Effect of cell configuration and fuel on SOFC modelling, *Proceedings of the 3rd International Symposium on Solid Oxide Fuel Cells, édité par Singhal et Iwahara, Honolulu (USA), Mai 16-21, 1993.*

[25] K. Nisancioglu & H. Karoliussen, Cell and Stack Optimisation by Modelling, *Actes du First European Solid Oxid Fuel Cells Forum, édité par U. Bossel, Lucerne, Suisse, Octobre 1994.*

[26] R. Ødegård, H. Karoliussen & K. Nisancioglu, Comparison of experimental results and a mathematical model for simulation of SOFC stack performance, *IEA Advanced Solid Oxide Fuel Cells, 6th Workshop and experts meeting, Rome, 1994.*

[27] S.V. Patankar, Numerical Heat Transfer and Fluid Flow, *Series in Computational Methods in Mechanics and Thermal Sciences, Minkowycz and Sparrow Eds., Mc Graw Hill, 1980.*

[28] Ch. Rechenauer, Dreidimensionale mathematische Modelliererung des stationären und instationären Verhaltens oxidkeramischer Hochtemperatur-Brennstoffzellen, *Ph. D. thesis, KFA Jülich, 1993.*

[29] J.R. Selman, How to model Solid Oxide Fuel Cells *Proc. of the International Energy Agency Workshop, Charmey, Switzerland, 1989.*

[30] A. Solheim, Proceedings of the Third International Symposium on Solid Oxide Fuel Cells, *Honolulu, Hawaii, The Electrochemical Society, Pennington, New Jersey, 1993.*

[31] C.G. Vayenas, S. Bebelis and S. Neophytides, Non-faradaic electrochemical modification of catalytic activity: partial oxidation of $C_2H_4$ on $Ag$ and $CH_3OH$ on $Pt$, *New Developments in Selective Oxidation, C. Conti and F. Trifiro eds., 643-652, 1990.*

# List of symbols

A anode

$c$ concentration, $mol\ m^{-3}$

C cathode

$\mathrm{Ch_a}$ air channel

$\mathrm{Ch_f}$ fuel channel

$C_{p_i}$, heat capacity of gas $i$, $kJkmol^{-1}\ K^{-1}$

$D_{i,mix}$ diffusion coefficient of species $i$ in the mixture

E electrolyte

$E$ activation energy, $kJ\ kg^{-1}\ K^{-1}$

$F$ Faraday constant, $A\ s\ mol^{-1}$

$h$ heat transfer coefficient, $W\ m^{-2}\ K^{-1}$

$\mathbf{j}$ electrical current, $mA\ cm^{-2}$

$K$ equilibrium constant,

$\mathbf{N_i}$ molar flux mol for species $i$, $mol\ s^{-1}$

$\mathbf{q}$ heat flux $W\ s^{-1}$

$T$ temperature, $K$

$Q$ heat source term, $W\ m^{-3}$

$Q_{chem}$ heat source term due to chemical reaction, $W\ m^{-3}$

$V$ velocity of the gas in the channels, $m\ s^{-1}$

$X_i$ molar concentration of species $i$

*Greek symbols*

$\Delta H$ enthalpy, $kJ$,

$\Delta S$ entropy, $kJK^{-1}$

$\Gamma_{\mathrm{Ch_a}}$ interface between air channel and solid walls

$\Gamma_{\mathrm{Ch_f}}$ interface between fuel channel and solid walls

$\lambda$ heat conductivity, $Wm^{-1}\ K^{-1}$

$\Phi$ electrical potential, $V$

$\rho$ electrical resistivity, $W^{-1}\ m\ K$

$\sigma$ electrical conductivity, $W\ m^{-1}\ K^{-1}$

$\Omega_S$ solid part of the physical domain

*Indices*

a air

f fuel

$i$ chemical species

$R$ reforming reaction

$S$ shift reaction